International Journal of Solids and Structures 49 (2012) 1421–1433

Contents lists available at SciVerse ScienceDirect

International Journal of Solids and Structures

journal homepage: www.elsevier.com/locate/ijsolstr

Homogenization methods to approximate the effective response of random fibre-reinforced Composites

Natasha Willoughby, William J. Parnell *, Andrew L. Hazel, I. David Abrahams

School of Mathematics, Alan Turing Building, University of Manchester, Oxford Road, Manchester M13 9PL, United Kingdom

ARTICLE INFO

Article history:
Received 5 July 2011
Received in revised form 2 February 2012
Available online 28 February 2012

Keywords:
Asymptotic homogenization
Fibre-reinforced composites
Microstructure
Representative volume element
Effective properties
Anisotropy

ABSTRACT

In this article a fibre-reinforced composite material is modelled via an approach employing a representative volume element with periodic boundary conditions. The effective elastic moduli of the material are thus derived. In particular, the method of asymptotic homogenization is used where a finite number of fibres are randomly distributed within the representative periodic cell. The study focuses on the efficacy of such an approach in representing a macroscopically random (hence transversely isotropic) material. Of particular importance is the sensitivity of the method to cell shape, and how this choice affects the resulting (configurationally averaged) elastic moduli. The averaging method is shown to yield results that lie within the Hashin–Shtrikman variational bounds for fibre-reinforced media and compares well with the multiple scattering and (classical) self-consistent approximations with a deviation from the latter in the larger volume fraction cases. Results also compare favourably with well-known experimental data from the literature.

1. Introduction

The study of materials possessing complex microstructure, and in particular those of a *host/inclusion* type where one material (the *inclusion phase*) is distributed inside another (the *host* phase), has become increasingly important in recent years due to the growing use of such media in applications (see e.g. Torquato, 2002; Guenneau et al., 2003; Smith and Pendry, 2006). Often the material in question possesses *periodic* microstructure, the periodicity and constituent materials being chosen so as to restrict the propagation of waves within certain frequency ranges (Guenneau et al., 2003; Parnell, 2007) and so as to create an induced anisotropy (Parnell and Abrahams, 2008a). In the low-frequency limit where the wavelength is much larger than the microstructural lengthscale, these materials possess *homogenized* material properties, i.e. the wavenumber lies inside the lowest pass band (excluding special cases such as high contrast media for example) and dispersion (frequency dependence) enters the problem at higher order. Classical asymptotic homogenization (Bakhvalov and Panasenko, 1989; Parton and Kudryavstev, 1993) can be used in this context. The two dimensional case (corresponding to fibre-reinforced composites where end effects of fibres are negligible) was considered for simple microstructures and elastostatics by Sabina et al. (2002) and references therein. For complex microstructures (several fibres of arbitrary cross section inside the periodic cell) the static (i.e. zero frequency) problem was considered by Greengard and Helsing (1998) and the low-frequency, elastodynamic regime was studied by Parnell and Abrahams (2006, 2008a). These models permit the effective material properties of the inhomogeneous medium to be determined via semi-analytical (multipole) methods based on complex variable theory. Other approaches that model periodic inhomogeneous media are the equivalent eigenstrain method (Nemat-Nasser and Hori, 1999), the method of cells (Aboudi, 1989) and the integral equation method (Parnell and Abrahams, 2008b).

Inhomogeneous media whose microstructure is *random* are less well understood because their effective behaviour depends strongly on the governing statistics of the random distribution. Effective properties may be determined by using the classical theory of multiple scattering in the low-frequency limit (see e.g. Bose and Mal, 1974a,b) which is attractive because this corresponds to the experimental determination of effective properties. In this analytical approach, averages of the governing field equations are taken and *closure approximations* are invoked, the most popular one being the Quasi-Crystalline Approximation (QCA) (Lax, 1952). Although closure schemes such as the QCA are attractive for their ease of use and the fact that they yield analytical results (Keller, 1962, pp. 228–229; Frisch, 1968, p. 188) the error induced by their implementation has never been fully understood. It is frequently claimed, for example, that the approximation is only valid for small volume fractions ϕ of the inclusion phase (Linton and Martin, 2004). In the low frequency limit however, the approximation gives results that are not inconsistent, in the sense that the predicted effective elastic properties reside inside strict variational

* Corresponding author.
E-mail address: William.Parnell@manchester.ac.uk (W.J. Parnell).

0020-7683/$ - see front matter © 2012 Elsevier Ltd. All rights reserved.
http://dx.doi.org/10.1016/j.ijsolstr.2012.02.010

bounds. They also give correct results as the volume fraction of the inclusion phase tends to 0 and 1 respectively (Bose and Mal, 1974a,b), i.e. they tend to the host and inclusion values respectively. Many alternative homogenization and micromechanical methods exist by which the effective properties of *random* inhomogeneous media can be determined. To name but a few we have, for example, the self-consistent schemes (Hill, 1965; Sabina et al., 1989; Kanaun and Levin, 2008a,b), the Mori–Tanaka method (Mori and Tanaka, 1973; Benveniste, 1987) and the differential scheme (Norris, 1985). These methods make simplified assumptions regarding the way that the phases interact on the microscale, but can often provide rapid and useful predictions of effective moduli. It is often difficult to assess their accuracy for a given volume fraction, especially in the (interesting and important) non-dilute regime.

An alternative low-frequency approach to determining the effective properties of random inhomogeneous media, which is becoming increasingly popular, is the so-called representative volume element (RVE) method. An RVE is defined as a region of the inhomogeneous material that should be large enough to be *representative* of the statistics of the material (Torquato, 2002; Ostoja-Starzewski, 2008) but small compared with the wavelength of the insonifying radiation. Effective properties for random media can be derived by solving *static boundary value problems* on the RVE and averaging the resulting fields over space and/or over configurations or 'realizations' as they are often called. Results from a true RVE should be independent of the chosen boundary conditions, but in reality the boundary conditions will always provide some influence on a finite domain. The notion is that provided the RVE is large enough, the resulting effective properties should be representative of the medium. A great deal of work has been undertaken to determine the appropriate *size* of an RVE, which depends on many factors such as microstructure lengthscale, phase properties (i.e. contrast) and geometry of the microstructure; see for instance Drugan and Willis (1996), Ostoja-Starzewski (1997), Kanit et al. (2003), Kaßbohm et al. (2006), Guilleminot et al. (2008) and Xu and Chen (2009) and references therein for further discussion.

RVE homogenization approaches fall into two camps. In both cases the first step is to choose the RVE size and shape, within which the microstructure of the medium is distributed. The two approaches vary in their choice of *boundary conditions*. The first approach applies specific macroscopic conditions on the boundary (usually those of homogeneous traction or displacement[1] since they satisfy the so-called Hill condition (Hill, 1963) and lead to simple expressions for, respectively, the average stress and strain fields in the composite). The respective average strain or stress fields are computed and the effective properties are thus determined. In this case the boundedness of the body influences the effective properties. The second approach (and the one that we employ in this paper) imposes *periodic* boundary conditions on the boundary of a tessellating domain (the periodic cell). The material can then be considered as one that is unbounded but represented by a periodic cell. Effective properties are then determined by any of the standard periodic homogenization methods for complex microstructure within the periodic cell, although very few existing methods can, in practice, deal with such complex geometries. In both approaches, configurational (or ensemble) averages over many realizations must be taken in order to determine the macroscopic effective properties of the medium under examination.

[1] Note that *homogeneous* boundary conditions here do *not* mean imposing $u_i = 0$ on the boundary for example in the context of displacement boundary conditions; it means $u_i = \overline{\varepsilon}_{ij} x_j$ on the boundary, where the components $\overline{\varepsilon}_{ij}$ are constant and as such they would yield uniform strains $\overline{\varepsilon}_{ij}$ in a homogeneous material. This terminology is standard in the homogenization and micromechanics community.

A comparison of the two RVE approaches for fibre-reinforced composites was provided by Trias et al. (2006) but this work mainly focused on their efficacy relating to damage prediction. A discussion of the advantages and disadvantages of the first approach is given by Huet (1990), Sab (1992) and Ostoja-Starzewski (1997). In particular these references describe how, by increasing the size of the RVE, the subsequent bounds on effective properties found by choosing both traction (lower bound) or displacement (upper bound) boundary conditions become tighter, with the characteristic size of the microscale being held fixed. These articles discuss static boundary value problems, but as described above when referring to the multiple scattering method, wave propagation can also be used to determine effective properties. Gomez Alvarez-Arenas et al. (2000) used a finite element method to simulate low frequency wave propagation in random, poly-disperse particulate composites. A single domain (RVE) is used and time-of-flight measurements are made on the wave-front propagation across the composite. Error bars indicate the level of uncertainty on the effective properties due to variations in microstructure.

The main problem with the finite domain RVE approach is the dependence on the boundary conditions chosen. No such problem exists with the second approach, but the fundamental flaw is that the material remains periodic and hence the resulting *macroscopic* field will be anisotropic in general, even when the periodic cell possesses complex microstructure. Hence the subsequent effective properties become dependent on the *shape* of the periodic cell. As with the first approach however, the RVE notion remains provided that there is enough statistical 'information' inside the cell and hence the effect of the periodicity is reduced. This approach has been implemented using classical homogenization by Byström (2003) in the context of electrostatics and Ghosh et al. (1995) for elastostatics. Baxter et al. (2001) used the method of cells for elastostatics, Gusev (1997) employed computational homogenization for three dimensional elastostatics, and Kanit et al. (2003) investigated the case of a polycrystal. Further, Gusev et al. (2000) used a Monte-Carlo approach to solve a periodic cell problem and energy methods to derive the effective elastic properties of a fibre-reinforced composite.

In the references just given, the choice of periodic cell is always a square (two dimensions) or cube (three dimensions) and hence if only one circular or spherical inclusion is placed inside these cells the resulting material would be tetragonal (6 elastic properties) and cubic (3 elastic properties) respectively. As the number of inclusions inside the periodic cell increases, the expectation is that the resulting (configurational averaged) elastic modulus tensor becomes transversely isotropic (5 elastic properties) and isotropic (2 elastic properties) in two and three dimensions respectively. Hence one of the key aspects of the periodic cell approach should be to investigate the induced *anisotropy* of the resulting averaged effective elastic modulus tensor for a fixed level of microstructure and in particular to assess whether cell shape affects the subsequent configurational averages. It is not self evident that the results for a square cell will be equivalent to those for a hexagonal cell, for instance. This notion was touched upon by Swaminathan et al. (2006) who tessellated the domain via a periodic but irregularly shaped cell and used this to investigate the effective elastic properties of fibre-reinforced composites. However this idea was not explored in any depth. It is a well-known result that when aligned fibres are positioned on a periodic *hexagonal* lattice the resulting material is *transversely isotropic*, i.e. it possesses the same elastic symmetry that a composite with truly randomly distributed aligned fibres would exhibit. Hence, even though in the past it appears that only square periodic cells have been chosen, a hexagonal cell may in fact be a more natural choice of shape to represent random fibre-reinforced media.

In this article we shall use classical asymptotic homogenization in the low frequency elastodynamic regime for fibre-reinforced materials (we consider circular cross section fibres only and these fibres are long, all aligned and made up of isotropic material) with complex microstructure in the periodic cell in order to assess the efficacy of the periodic RVE approach. In particular, this allows us to use the concise expressions derived by Parnell and Abrahams (2006, 2008a) for the effective elastic properties of a fibre-reinforced material with complex microstructure. We are specifically interested in exploring the effect of periodic cell *shape* and in making comparisons with other homogenization schemes and experimental results. Specifically, we aim to address the following issues in order to determine the properties that a periodic cell must possess so that it can be defined as a representative volume element (RVE):

(1) For a given number of fibres, say N, in the periodic cell, how many distinct configurations M are required to obtain a fully converged average field?
(2) (a) Given a specific cell shape and volume fraction ϕ of fibre material, how do configurational averaged effective properties depend on the number N of fibres within the cell?
(b) Given any number $N > 1$ of fibres within the periodic cell, will the resulting configurational averaged elastic modulus tensor be transversely isotropic?
(c) How many fibres are necessary for a *single configuration* (rather than a configurational average) to be a reasonable approximation to a transversely isotropic medium, given some specified 'tolerance'?
(3) How do the effective properties depend on periodic cell shape?
(4) How do the predictions from the periodic cell approach compare with other homogenization methods?

Note that we take fibres of circular shape only, and fibres which are all of the same size and material parameters i.e. mono-disperse fibre-reinforced composites, because consideration of such composites allows us to answer the questions that we have posed above without adding extraneous detail.

In Section 2 we will summarise the results derived by Parnell and Abrahams (2006, 2008a), providing expressions for the effective properties of a monoclinic fibre-reinforced medium. These expressions are functions of the solution to the periodic cell problem. This cell problem is summarised in Section 3 and we describe two approaches to determining its solution: a multipole method using doubly periodic functions and a numerical approach using a finite element method. In Section 4 we describe our results and findings and in particular we discuss the notion of *cell shape dependence* for the periodic cell approach. We close in Section 5 with conclusions.

2. Homogenization of fibre-reinforced composites with complex microstructure

We first briefly summarise the main results from the articles by Parnell and Abrahams (2006, 2008a), in which expressions were derived for the effective properties of a periodic fibre-reinforced composite where the periodic cell contains N identical fibres arbitrarily distributed inside a host phase. From the outset we consider fibres of *circular* cross section only and isotropic phases and note that, for a given general configuration of N arbitrarily distributed fibres inside the periodic cell, this results in a macroscopically *monoclinic* material having elastic symmetry with respect to one plane only; therefore, there are 13 independent effective elastic moduli (Parnell and Abrahams, 2008a).

2.1. The homogenized wave equation

We work in Cartesian coordinates $\hat{\mathbf{x}} = (\hat{x}_1, \hat{x}_2, \hat{x}_3)$, where a *hat* denotes a dimensional variable, and we take the fibres to be of infinite extent and aligned in the $\hat{x}_3$ direction. Thus, the material can essentially be considered as two-dimensional (end effects of the fibres are neglected) and we need only consider the cross section in the $\hat{x}_1\hat{x}_2$ plane. Furthermore, since it is periodic the microstructure is defined by a periodic cell which tessellates this plane. Fig. 1 illustrates several examples of the cross section of a periodic fibre-reinforced composite material with complex microstructure.

We define the centre[2] of the (s,t)th periodic cell as

$$\hat{\mathbf{R}}(s,t) = q(s\mathbf{l_1} + t\mathbf{l_2}), \quad s,t \in \mathbb{Z}, \tag{2.1}$$

where q is the characteristic lengthscale of the periodic cell and hence the microstructure, and $\mathbf{l_1}, \mathbf{l_2} \in \mathbb{R} \times \mathbb{R}$ are vectors whose components are $O(1)$. With reference to Fig. 1, a typical periodic cell is made up of a *host phase* occupying domain D_0 with area $|D_0|$, and mass density $\hat{\rho}_0$. Embedded in the host phase in the periodic cell are the randomly distributed *inclusions* - in this case N identical fibres with domains $D_1, D_2, \ldots, D_r, \ldots, D_N$. Their areas are denoted by $|D_r| = \pi a^2,\ r = 1,2,\ldots,N$, where a is their radius and they each have mass density $\hat{\rho}_1$. The general theory permits fibres of arbitrary cross section to be considered, although here for ease of exposition we shall consider the case of circular cross sections only; the boundary of the rth fibre being denoted by ∂D_r.

We consider the propagation of low-frequency linear elastic waves in the $\hat{x}_1\hat{x}_2$ plane. Therefore, horizontally polarized shear (SH) waves are polarized along the $\hat{x}_3$ axis (in the direction of the fibres), and longitudinal/vertically polarized shear (P/SV) waves are polarized in the $\hat{x}_1\hat{x}_2$ plane. We assume time harmonic motion, with behaviour $\exp(-i\omega t)$, so that Navier's equations for the displacements $\hat{u}_i(\hat{\mathbf{x}})$ are, in general,

$$\frac{\partial}{\partial \hat{x}_j}\left(\hat{C}_{ijkl}(\hat{\mathbf{x}})\frac{\partial \hat{u}_k(\hat{\mathbf{x}})}{\partial \hat{x}_l}\right) + \omega^2\hat{\rho}(\hat{\mathbf{x}})\hat{u}_i(\hat{\mathbf{x}}) = 0, \tag{2.2}$$

in which the mass density $\hat{\rho}$ and the elastic modulus tensor $\hat{C}_{ijkl}$ are henceforth taken as piecewise constant functions of $\hat{\mathbf{x}}$ reflecting the host/fibre microstructure, with all fibres having identical properties. The host has density $\hat{\rho}_0$ and Lamé moduli λ_0, μ_0 whilst the fibres have density $\hat{\rho}_1$ and moduli λ_1, μ_1. From a notational viewpoint it is convenient to work with the isotropic tensor $\hat{C}^r_{ijkl},\ r = 0,1,\ldots,N$, in the form

$$\hat{C}^r_{ijkl} = [\lambda_1 + (\lambda_0 - \lambda_1)\delta_{r0}]\delta_{ij}\delta_{kl} + [\mu_1 + (\mu_0 - \mu_1)\delta_{r0}](\delta_{ik}\delta_{jl} + \delta_{il}\delta_{jk}). \tag{2.3}$$

We now nondimensionalize based on the properties of the host material, i.e. $\rho^r = \hat{\rho}/\hat{\rho}_0,\ \hat{u}_i = \hat{U}u_i$ (where $\hat{U}$ is a typical displacement magnitude), $\hat{\mathbf{x}} = q\mathbf{x}$ and $C^r_{ijkl} = \hat{C}^r_{ijkl}/\hat{C}^0_{1212} = \hat{C}^r_{ijkl}/\mu_0$, where

$$\rho^r = \hat{\rho}_1/\hat{\rho}_0 + (1 - \hat{\rho}_1/\hat{\rho}_0)\delta_{r0}, \tag{2.4}$$

and (2.3) becomes

$$C^r_{ijkl} = [p_1 + (p_0 - p_1)\delta_{r0}]\delta_{ij}\delta_{kl} + [m_1 + (1 - m_1)\delta_{r0}](\delta_{ik}\delta_{jl} + \delta_{il}\delta_{jk}), \tag{2.5}$$

in which $p_r = \lambda_r/\mu_0$ and $m_r = \mu_r/\mu_0$. Hence, the governing Eq. (2.2) simplifies to

$$\frac{\partial}{\partial x_j}\left(C^r_{ijkl}\frac{\partial u_k(\mathbf{x})}{\partial x_l}\right) + \epsilon^2\rho^r u_i(\mathbf{x}) = 0. \tag{2.6}$$

Here we have defined

[2] Here the *centre* of the periodic cell is taken as any convenient point.

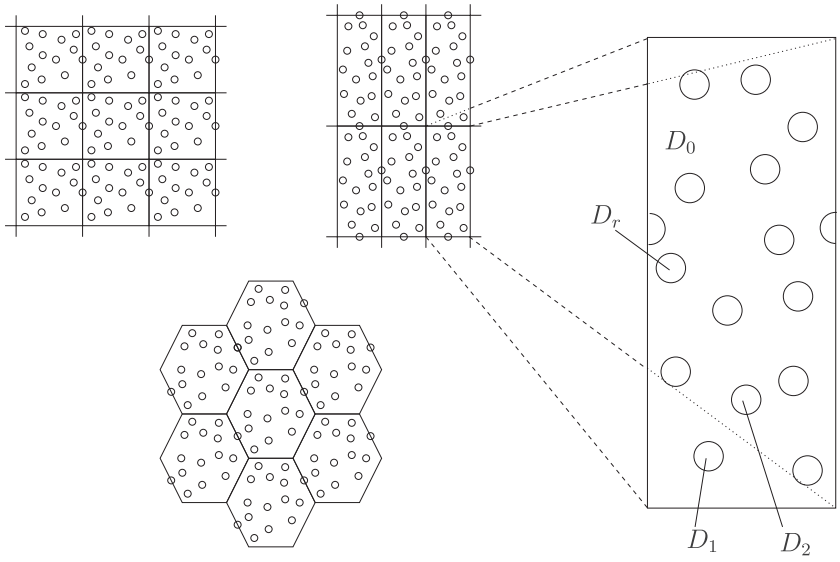

Fig. 1. Figure illustrating several examples of periodic cells; in this case, square, rectangular and hexagonal and a close-up of the rectangular periodic cell.

$$\epsilon = qK_0 \ll 1, \tag{2.7}$$

the small parameter in our asymptotic analysis, reflecting the fact that the elastic wavelengths are much longer than the characteristic lengthscale of the periodic cell. Furthermore, $K_0^2 = \omega^2\hat{\rho}_0/\hat{C}^0_{1212}$ is a representative wavenumber of the medium, associated with shear waves in the host phase. We could instead rescale on the longitudinal wavenumber, but we assume that there will always be a separation-of-scales in the material, allowing us to use asymptotic homogenization and hence this choice is immaterial. In nondimensionalized variables, the lattice vector (2.1) becomes $\mathbf{R}(s,t) = s\mathbf{l_1} + t\mathbf{l_2},\ s,t \in \mathbb{Z}$.

We assume perfect bonding at the fibre/host interfaces, so that boundary conditions on ∂D_r are continuity of displacement and continuity of normal stress:

$$u_i(\mathbf{x})|_{\partial D_r^+} = u_i(\mathbf{x})|_{\partial D_r^-}, \tag{2.8}$$

$$C^0_{ijkl}\frac{\partial u_k}{\partial x_l}(\mathbf{x})n_j^r\Big|_{\partial D_r^+} = C^r_{ijkl}\frac{\partial u_k}{\partial x_l}(\mathbf{x})n_j^r\Big|_{\partial D_r^-}, \tag{2.9}$$

for $i = 1,2,3$ and $r = 1,2,\ldots,N$, where n_j^r is the jth component of the (outward pointing) normal to the boundary ∂D_r of the rth fibre. The notation ∂D_r^+ or ∂D_r^- denotes the boundary ∂D_r approached from inside D_0 and inside D_r respectively.

The method of asymptotic homogenization (Bakhvalov and Panasenko, 1989; Parton and Kudryavtsev, 1993) proceeds by defining the two (assumed independent) lengthscales

$$x_\alpha = \xi_\alpha, \quad \alpha = 1,2, \qquad x_k = \frac{1}{L(\epsilon)}z_k, \quad k = 1,2,3, \tag{2.10}$$

where here and throughout, Greek indices indicate an index that can run over 1 and 2 only, and Latin indices represent an index that can run over 1, 2 and 3. $L(\epsilon)$ is an expansion in ϵ, which tends to zero as $\epsilon \to 0$. The variables $\boldsymbol{\xi} = (\xi_1, \xi_2)$ and $\mathbf{z} = (z_1, z_2, z_3)$ are short and long lengthscales respectively, and we note that $\boldsymbol{\xi}$ has no component in the x_3 direction since there is no microstructural variation in that direction. Displacements $u_k(\mathbf{x})$ are now taken to depend on the two independent variables $\boldsymbol{\xi}$ and $\mathbf{z}$, i.e. $u_k(\mathbf{x}) = u_k(\boldsymbol{\xi}, \mathbf{z})$ and since the elastic moduli and mass density vary only on the microscale then we have $\rho^r = \rho(\boldsymbol{\xi})$ and $C^r_{ijkl} = C_{ijkl}(\boldsymbol{\xi})$.

We assume asymptotic expansions of the displacements and $L(\epsilon)$ in powers of ϵ, and use these together with multiple scales expansions of the derivatives in (2.6)–(2.9). Equating terms of the same order in ϵ yields a hierarchy of problems. It can be shown that (Parnell and Abrahams, 2008a) the resulting homogenized wave equation for the leading order term in the expansion of the displacement $U_i = U_i(\mathbf{z})$ (i.e. the *homogenized* solution as $\epsilon \to 0$) is

$$C^*_{ijpm}\frac{\partial^2 U_p}{\partial z_j \partial z_m} + \rho^* U_i = 0, \tag{2.11}$$

where

$$C^*_{ijpm} = p_A\delta_{ij}\delta_{pm} + m_A(\delta_{ip}\delta_{jm} + \delta_{im}\delta_{jp}) + S_{pm}\delta_{ij} + T_{i\beta pm}\delta_{j\beta} + T_{j\beta pm}\delta_{i\beta}, \tag{2.12}$$

in which

$$S_{pm} = (p_1 - p_0)\sum_{r=1}^{N} H^r_{\beta\beta pm}, \quad T_{i\beta pm} = (m_1 - 1)\sum_{r=1}^{N} H^r_{i\beta pm}, \tag{2.13}$$

and

$$H^r_{k\beta pm} = \frac{1}{|D|}\int_{\partial D_r} N^r_{kpm}(\boldsymbol{\xi})n^r_\beta \,\mathrm{d}l. \tag{2.14}$$

The tensor N^r_{kpm} is the (doubly periodic) solution to the so-called (p,m)th *cell problem* $(p,m = 1,2,3)$, which always arises in asymptotic homogenization, and $|D| = \sum_{r=0}^{N}|D_r|$ is the area of the fundamental cell (as it is a sum over all the phases in the periodic cell). The effective elastic moduli C^*_{ijpm} are therefore defined in terms of the solutions to these cell problems, which are discussed in the following Section. In (2.12) the subscript A denotes the arithmetic average, i.e.

$$p_A = (1-\phi)p_0 + \phi p_1, \quad m_A = (1-\phi) + \phi m_1, \tag{2.15}$$

where ϕ is the volume fraction of the fibres, i.e. $\phi = N\pi a^2/|D|$ and a is the radius of each fibre. The effective mass density of the periodic cell is $\rho^* = \rho_A$. Finally, we note that the tensor $H^r_{k\beta pm}$ accounts for the induced anisotropy due to the presence of aligned fibres.

Before examining the fundamental cell problem, it is worth briefly stating the form that the effective elastic modulus tensor will take for single configurations, and for averaged configurations.

2.2. Monoclinic media

Given one configuration (i.e. one specific distribution of N fibres within the periodic cell), and each phase being isotropic, then the

material has effective modulus tensor C^*_{ijkl} defined by (2.12) and this is monoclinic, having 13 independent components. This can be seen by comparing Navier's equations for a monoclinic material with effective equations (2.11) and (2.12) (see Parnell and Abrahams (2008a)).

For the purposes of this study we can confine our attention to just *six* components of the effective modulus tensor

$$C^*_{1111} = c^*_{11} = p_A + 2m_A + S_{11} + 2T_{1111}, \tag{2.16}$$
$$C^*_{2222} = c^*_{22} = p_A + 2m_A + S_{22} + 2T_{2222}, \tag{2.17}$$
$$C^*_{1212} = c^*_{66} = m_A + T_{1212} + T_{2112}, \tag{2.18}$$
$$C^*_{1122} = c^*_{12} = p_A + S_{11} + 2T_{2211} = p_A + S_{22} + 2T_{1122}, \tag{2.19}$$
$$C^*_{3232} = c^*_{44} = m_A + T_{3232}, \tag{2.20}$$
$$C^*_{3131} = c^*_{55} = m_A + T_{3131}, \tag{2.21}$$

where c^*_{ij} is the effective modulus tensor in *engineering* notation. We remind the reader that all effective moduli are scaled on the host shear modulus, $\hat{C}^0_{1212} = \hat{c}^0_{66} = \mu_0$.

2.3. Random media: transverse isotropy

A fibre-reinforced material in which the fibres are truly randomly distributed over all space (in the x_1x_2 plane) is transversely isotropic on the macroscale; it therefore possesses five elastic constants. In this case we must have $c^*_{16} = c^*_{26} = c^*_{36} = c^*_{45} = 0$ and the relationships

$$c^*_{11} = c^*_{22}, \quad c^*_{13} = c^*_{23}, \tag{2.22}$$
$$c^*_{66} = \frac{1}{2}(c^*_{11} - c^*_{12}), \quad c^*_{44} = c^*_{55}. \tag{2.23}$$

As we shall see later, we will perform ensemble averaging over many configurations of monoclinic media with the periodic structure described above (N fibres in the cell), in order to assess in what sense the configurationally averaged material properties can be considered to be a good approximation to a transversely isotropic material.

3. The cell problems and their solution

The so-called (p,m)th cell problem which must be solved for the doubly-periodic functions $N_{kpm}(\boldsymbol{\xi}) = N_{kpm}(\boldsymbol{\xi} + \mathbf{R})$ appearing in (2.14) can be summarised in the following manner. Firstly, we suppress the explicit dependence on the subscripts p, m, which remain fixed in each cell problem, by using a bold font to denote any quantity with p, m subscripts; in other words, the quantity $\mathbf{N}_i$ represents N_{ipm}. The governing equations for $\boldsymbol{\xi} \in D_r$ are then (Parnell and Abrahams (2008a))

$$\frac{\partial}{\partial \xi_\alpha}\left(C^r_{i\alpha k\beta}\frac{\partial \mathbf{N}^r_k}{\xi_\beta}\right) = 0 \tag{3.1}$$

with associated boundary conditions

$$\mathbf{N}^0_i\Big|_{\partial D^+_r} - \mathbf{N}^r_i\Big|_{\partial D^-_r} = 0, \tag{3.2}$$
$$\left(C^0_{i\alpha k\beta}\frac{\partial \mathbf{N}^0_k}{\partial \xi_\beta}\Big|_{\partial D^+_r} - C^r_{i\alpha k\beta}\frac{\partial \mathbf{N}^r_k}{\partial \xi_\beta}\Big|_{\partial D^-_r}\right) n^r_\alpha = \mathbf{F}^r_{i\alpha} n^r_\alpha, \tag{3.3}$$

where

$$\mathbf{F}^r_{i\alpha} \text{ represents } F^r_{i\alpha pm} = C^r_{i\alpha pm} - C^0_{i\alpha pm}. \tag{3.4}$$

For isotropic and transversely isotropic phases the anti-plane problem ($i = 3$) decouples from the in-plane problem ($i = 1, 2$).

In Parnell and Abrahams (2006, 2008a) complex variable theory was employed in order to solve the cell problems described above for isotropic phases. Doubly-periodic multipole expansions were written down and the only numerical computation involved was the solution of a dense linear system of equations for the unknown coefficients in these expansions. The method is very efficient for small numbers of fibres or for dilute concentrations, e.g. $\phi < 0.05$ when only three terms are required in the multipole expansion for moderate to large N. In the current context we wish to investigate many realizations with large numbers of fibres and moderate to high volume fractions ϕ, which requires many terms in the multipole expansions. The increasing size of the dense linear system renders the method extremely expensive computationally.

As an alternative, we can solve the cell problem using a finite element method, which results in a large but sparse linear system of equations. The method is based on the weak form of the governing equation (3.1), obtained by multiplication of the equation by a suitable test function $v(\boldsymbol{\xi})$, integration over the unit cell and use of the divergence theorem. In each domain D_r, the weak form is

$$\iint_{D_r}\left(C^r_{i\alpha k\beta}\frac{\partial \mathbf{N}^r_k}{\partial \xi_\beta}\right)\frac{\partial v}{\partial \xi_\alpha}\,\mathrm{d}D = \oint_{\partial D_r}\left(C^r_{i\alpha k\beta}\frac{\partial \mathbf{N}^r_k}{\partial \xi_\beta}\,v\right)n^r_\alpha\,\mathrm{d}l, \tag{3.5}$$

and the problem is forced by the traction applied at the boundary, the right-hand side of (3.5). The jump in traction between domains is given by the boundary condition (3.3), which can be directly incorporated into the weak form by imposing

$$\iint_{D_r}\left(C^r_{i\alpha k\beta}(\boldsymbol{\xi})\frac{\partial \mathbf{N}^r_k}{\partial \xi_\beta}\right)\frac{\partial v}{\partial \xi_\alpha}\,\mathrm{d}D + \oint_{\partial D_r} C^r_{i\alpha pm} n^r_\alpha v\,\mathrm{d}l = 0. \tag{3.6}$$

Each fibre domain and the host phase domain is discretised by isoparametric quadratic nodal triangular finite elements using the Triangle (Shewchuk, 1996) mesh generator. The displacement boundary condition (3.2) is satisfied by ensuring that all neighbouring elements, including those in different domains and those across the boundaries of the periodic cell, are conforming, i.e. the nodal positions and corresponding displacement components are identical on the common boundaries, or, equivalently, nodes are *shared* between neighbouring elements. The boundary condition (3.3) will be correctly imposed provided that each physical fibre boundary is included twice: once as a fibre boundary and once as a boundary of the host phase, with the accompanying change in sign of the outward unit normal.

A Galerkin method is used to obtain a global system of discrete linear equations from Eq. (3.6), so the test functions are chosen to be identical to the quadratic basis functions used to approximate the unknown displacement components. The resulting linear system is assembled and solved using the OOMPH-LIB finite element library (Heil and Hazel, 2006) and the SuperLU direct linear solver Demmel et al. (1999). Note that the six different combinations of (p,m) required for the determination of c^*_{ij} change only the forcing vector on the right-hand side of the linear system and so all problems can be solved by a single LU factorisation followed by six back-substitution steps.

Each realization of the cell problem, corresponding to a given number of fibres and volume fraction, is generated by randomly choosing the ξ_1 and ξ_2 coordinates of each fibre centre from a suitable uniform distribution. Fibres are not permitted to intersect but they may cross the boundaries of the periodic cell.

4. Results and discussion

Throughout this Section we shall focus on results associated with a glass–epoxy fibre-reinforced composite material (glass fibres distributed inside the epoxy host phase). The glass phase has Young's modulus $E_1 = 73.1$ GPa and Poisson's ratio $\nu_1 = 0.22$ whereas the epoxy phase has $E_0 = 3.45$ GPa and $\nu_0 = 0.35$. These correspond to Lamé moduli $\mu_0 = 1.3$ GPa, $\mu_1 = 30$ GPa, $\lambda_0 = 3$ GPa, $\lambda_1 = 23.5$ GPa.

4.1. A comparison of the cell solution methods

In order to give confidence in the two alternative solution approaches to the cell problem we compare resulting effective moduli obtained by the multipole method and the FE scheme for small N. In Table 1 we show results, correct to 3 decimal places for selected elastic moduli associated with a specific 'typical' configuration (given in Fig. 2) and the time taken to achieve these results. As seen, the two approaches yield the same effective moduli (and this is true for the remaining elastic constants). For these results we consider a *square* periodic cell and volume fractions $\phi = 0.05$ and 0.25, respectively, of the glass fibre phase. Typical configurations for $N = 1, 4, 10$ are shown in Fig. 2. Configurations are constructed by first choosing N and ϕ and successively choosing random points within the cell (corresponding to the fibre centres) such that the fibres do not overlap.

Note that the two methods yield similar results for the elastic moduli for other shapes of periodic cell. As expected, the time taken for solution increases with N since the system size also increases. The evaluation time also increases with increasing ϕ; for the FE method this is because more elements are required, particularly around fibre boundaries, to achieve the same resolution. For the multipole approach this is because a larger number of terms are required in the multipole expansion and hence the (dense) linear system increases in size. As expected, the multipole method is quicker than the FE scheme for $\phi \ll 1$ with $N = 1$, but the relative increase in cost of the FE method with increasing ϕ and N is much less than that of the multipole method. Thus, for larger ϕ and N the FE method is significantly faster. Although the multipole method is a perfectly feasible solution method to use for $N < 10$ say, the speed of the FE approach motivates its use for $N \gg 1$ in what follows.

4.2. The effects of configuration

For a given number of fibres N and volume fraction ϕ the effective properties of the resulting composite will be different for each possible configuration of the fibres. To discuss the *average* properties of such media, we define the *configurational* (or ensemble) average of the effective elastic moduli by

$$\langle c^*_{ij}\rangle^N_M = \frac{1}{M}\sum_{m=1}^{M} c^{*m}_{ij}, \tag{4.1}$$

where N is the number of fibres in the periodic cell, c^{*m}_{ij} is the (i,j)th effective elastic modulus for configuration m, and M is the number of configurations over which we average.

Of course, the average over a finite number of realizations is only ever an approximation to the *true* configurational average over every possible realization. Nonetheless, we expect that increasing the number of finite realizations will result in the approximate average (4.1) converging to the true configurational average. Moreover, any sufficiently large number of configurations should approximate the true configurational average to a particular accuracy. Our aim is to find the value of M to achieve our chosen accuracy. Table 2 shows ensemble averaged elastic moduli for four different start seeds[3] $S_j, j = 1,2,3,4$ used to generate four sets of $M = 1000$ different configurations in the case of $\phi = 0.15, N = 16$ and $N = 64$ over a hexagonal cell. When $N = 16$, it appears that we have achieved convergence (in a configurational average sense) to two decimal places; to obtain *three* decimal places we would need an average over a larger number of configurations. When $N = 64$, the Table shows that the different start seeds gives $\langle c_{44}\rangle_{1000}$ and $\langle c_{66}\rangle_{1000}$ to three decimal places; $\langle c_{11}\rangle_{1000}$ is still only accurate (in a configurational average sense) to 2 decimal places however. Thus, given some specified 'configurational average tolerance', the required M will be different for each modulus and will also depend upon ϕ, N and the cell shape.

We now consider the convergence of the configurational average results with increasing M and N. For definiteness let us focus our attention on the case when $\phi = 0.15$. For larger ϕ we expect that M will be larger in order to achieve the same degree of accuracy, or convergence of the average defined in (4.1). We shall consider the cases of square, hexagonal and rectangular cell shapes and $N = 2, 4, 16$ and 64. As noted above, the value of M required for a given configurational averaged accuracy is different for each of the individual elastic moduli. For example c^*_{33} typically requires only $M = O(10)$, whereas c^*_{11} needs $M = O(10^3)$ to obtain the same level of accuracy. In Fig. 3 we plot $\langle c^*_{55}\rangle$ as a function of M for a rectangular cell; as N increases, we observe faster convergence to the limiting configurational average value. In other words, the anisotropy induced by a small number of large fibres is larger than a large number of small fibres. If we magnified each of the graphs we would see that for $N = 2$ the average has barely converged to 3 decimal places by $M = 1000$ whereas for $N = 4$ the results have converged to 3 decimal places by $M \sim 700$. For $N = 16$ we need $M \sim 500$ and for $N = 64$ we need $M \sim 350$.

Table 1
Comparison of timings of the Multipole and FE methods to solve the cell problem at $\phi = 0.05$ and 0.25 for the square cell configuration shown in Fig. 2. All results for c^*_{ij} in the Table are accurate to 3 decimal places and are independent of the numerical method employed. Approximate times (averaged over 3 configurations) in seconds taken to obtain the results are also shown.

	$N = 1$		$N = 4$		$N = 10$	
c^*_{ij}	$\phi = 0.05$	$\phi = 0.25$	$\phi = 0.05$	$\phi = 0.25$	$\phi = 0.05$	$\phi = 0.25$
c^*_{11}	4.593	6.181	4.586	6.391	4.592	6.145
c^*_{12}	2.427	2.929	2.423	2.857	2.430	3.020
c^*_{44}	1.096	1.596	1.105	1.579	1.096	1.658
c^*_{66}	1.076	1.407	1.073	1.405	1.080	1.484
Time (s)						
Multi	1.08	1.08	12.02	75.28	83.39	455.71
FE	1.86	2.14	4.63	7.27	5.58	16.22

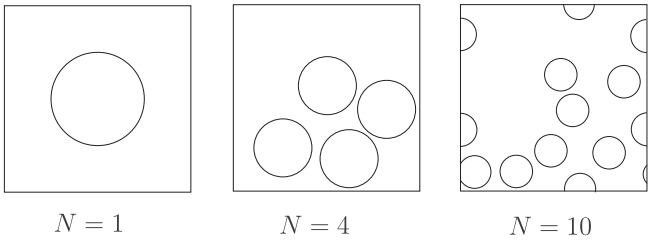

Fig. 2. A typical configuration in a square periodic cell with $N = 1, 4$ and 10 $\phi = 0.25$. Corresponding results for some of the effective moduli are given in Table 1.

Table 2
Given four different start seeds S_j, $j = 1,2,3,4$, we tabulate results of the configurational averages $\langle c^*_{11}\rangle^N_{1000}$, $\langle c^*_{44}\rangle^N_{1000}$, $\langle c^*_{66}\rangle^N_{1000}$ for $N = 16$ and $N = 64$, over a hexagonal periodic cell with $\phi = 0.15$.

Seed	$\langle c^*_{11}\rangle^{16}_{1000}$	$\langle c^*_{11}\rangle^{64}_{1000}$	$\langle c^*_{44}\rangle^{16}_{1000}$	$\langle c^*_{44}\rangle^{64}_{1000}$	$\langle c^*_{66}\rangle^{16}_{1000}$	$\langle c^*_{66}\rangle^{64}_{1000}$
S_1	5.27087	5.27215	1.33310	1.33414	1.27878	1.27916
S_2	5.27079	5.27270	1.33372	1.33388	1.27875	1.27923
S_3	5.27292	5.27254	1.33284	1.33384	1.27855	1.27933
S_4	5.27098	5.27152	1.33333	1.33435	1.27828	1.27941

[3] We note that a start seed is a numerical way to generate random data (here random positions of fibres within the cell) which can then be regenerated by using the same start seed in the future. This enables repeatable numerical experiments with random data.

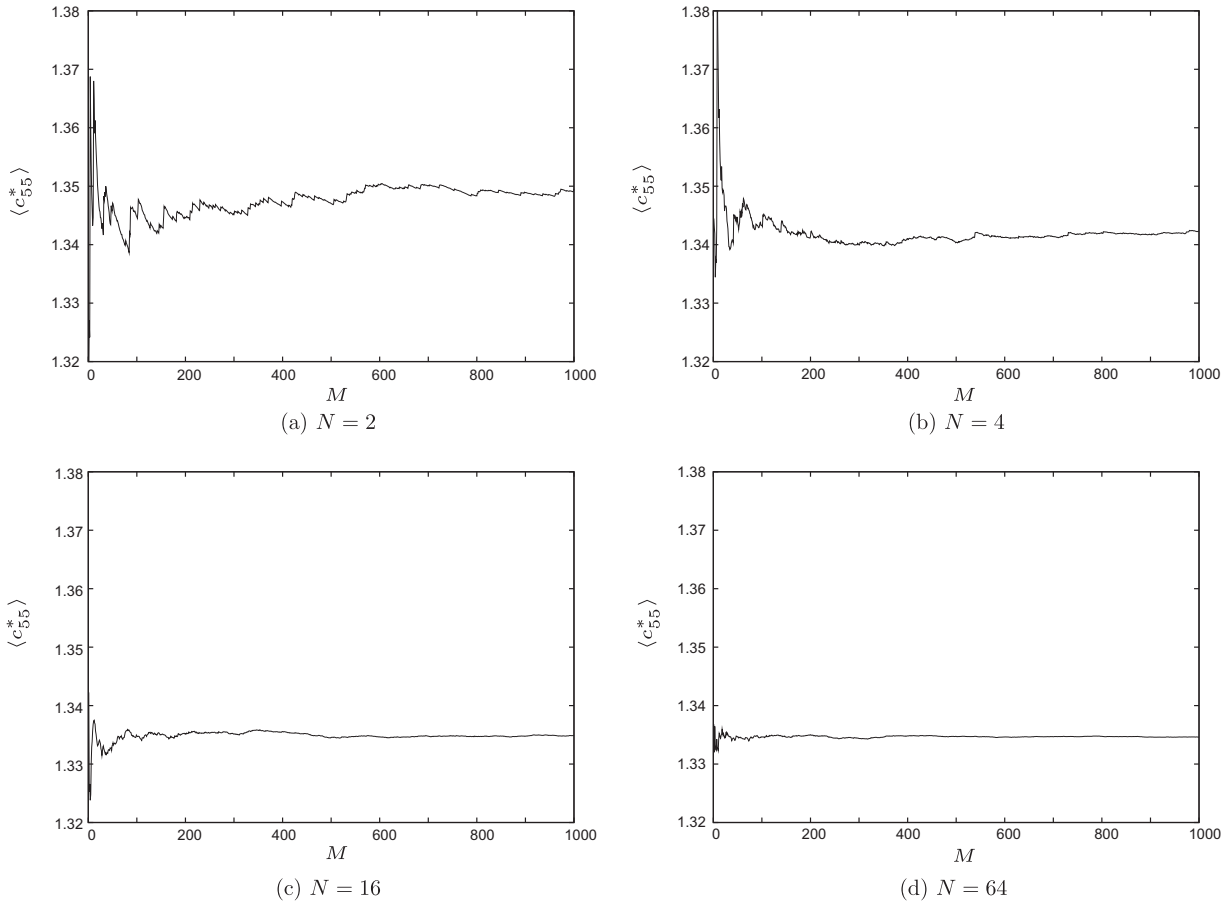

(a) $N = 2$ (b) $N = 4$ (c) $N = 16$ (d) $N = 64$

Fig. 3. Figure to show how the configurational average $\langle c^*_{55} \rangle$ develops for different N for a rectangular periodic cell with volume fraction $\phi = 0.15$.

Of the three cell shapes considered, convergence is slowest for the rectangular cell because, for a given N, it can induce larger anisotropy than the hexagon and square cases. Thus, a larger number of configurations are required in order to average out this anisotropy. The average elastic moduli associated with both the square and hexagonal shapes converge at approximately the same rate, with the hexagonal cell being marginally quicker.

We have conducted a large number of similar calculations and found that for any given start seed, and hence any set of configurations, when $\phi = 0.15$, $M \sim 100$ gives configurational-averaged convergence to 2 decimal places for all elastic moduli whilst taking $M \sim 1000$ ensures configurational-averaged convergence to 3 decimal places for all moduli except $\langle c_{11} \rangle$ which appears to require $M = O(10^4)$. We have thus answered question (1) posed in the introduction. In what follows then, in the main we focus on $\langle c_{44} \rangle^N_{1000}$, $\langle c_{55} \rangle^N_{1000}$ and $\langle c_{66} \rangle^N_{1000}$ since we know that in terms of a configurational average we have accuracy at $\phi = 0.15$ to 2 decimal places ($N = 16$) and 3 decimal places ($N = 64$).

4.3. Dependence of effective properties on N

We are now in a position to address questions (2a) and (2b) of the introduction. We shall present results mainly for a hexagonal periodic cell and a fibre volume fraction of $\phi = 0.15$. The same qualitative trends are found for any combination of cell shape and volume fraction.

To begin our consideration of question (2a) we refer back to Fig. 3 for a rectangular periodic cell, which shows that $\langle c^*_{55} \rangle$ does not converge to the same value for different N, but for increasing N, each successive $\langle c^*_{55} \rangle$ approximation gets closer in value. For a hexagonal periodic cell for fixed $\phi = 0.15$ we plot in Fig. 4 the configurational average $\langle c^*_{66} \rangle^N_{1000}$ for fibre numbers $N = 1, 4, 16, 64$. Also shown on this Figure, in a similar fashion to that given in Gusev (1997), are vertical bars corresponding to the difference between respective values of $\langle c^*_{66} \rangle^N_{1000}$; these clearly indicate the very rapid convergence of this configurational average to a finite value, shown by the dashed line, as $N \to \infty$. In fact, this is true for any other sequence of increasing N values that we might consider, and we confirm results in the previous section that $\langle c^*_{66} \rangle^{64}_{1000}$ is accurate (in the sense of a configurational average) within graphical tolerance, i.e. to three decimal places. Thus, we conclude that the ensemble averaged properties do depend on N, but for sufficiently large N they are constant to a given accuracy.

For large enough M, the configurational-averaged modulus $\langle c^*_{ij} \rangle^N_M$ converges to some constant value within a specified tolerance for any i, j, N. We now turn our attention to question (2b) which asks if there is some $N > 1$ such that the tensor $\langle c^*_{ij} \rangle^N_M$ is transversely isotropic (henceforth referred to as TI), with respect to some measure? If the configurational averages of the elastic moduli are TI, then, from Section 2.3, we must have

$$\langle c^*_{66} \rangle = \frac{1}{2}(\langle c^*_{11} \rangle - \langle c^*_{12} \rangle), \tag{4.2}$$

$$\langle c^*_{11} \rangle = \langle c^*_{22} \rangle, \tag{4.3}$$

$$\langle c^*_{44} \rangle = \langle c^*_{55} \rangle, \tag{4.4}$$

$$\langle c^*_{13} \rangle = \langle c^*_{23} \rangle. \tag{4.5}$$

We thus define the following relative errors associated with the mth configuration:

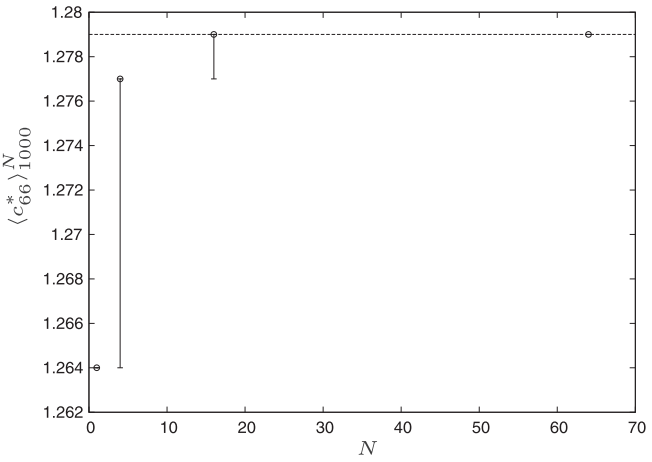

Fig. 4. For a hexagonal periodic cell for fixed $\phi = 0.15$, the configurational average $\langle c^*_{66}\rangle^N_{1000}$ is plotted for fibre numbers $N = 1, 4, 16, 64$. The difference between consecutive values is shown by the vertical bars. As N increases $\langle c^*_{66}\rangle^N_{1000}$ converges towards a value which is shown by the dashed line.

$$e^m_{66} = \frac{c^{*m}_{66} - 0.5(c^{*m}_{11} - c^{*m}_{12})}{c^{*m}_{66}}, \quad e^m_{11} = \frac{c^{*m}_{11} - c^{*m}_{22}}{c^{*m}_{11}}, \tag{4.6}$$

$$e^m_{44} = \frac{c^{*m}_{44} - c^{*m}_{55}}{c^{*m}_{44}}, \quad e^m_{13} = \frac{c^{*m}_{13} - c^{*m}_{23}}{c^{*m}_{13}}, \tag{4.7}$$

which give a measure of how close the mth configuration is to being TI. We define the mean of the relative errors $\langle e_{ij}\rangle^N_M$ for a set of M configurations by

$$\langle e_{ij}\rangle^N_M = \frac{1}{M}\sum_{m=1}^{M} e^m_{ij}. \tag{4.8}$$

For our purposes, the mean absolute relative error defined as

$$\langle d_{ij}\rangle^N_M = \frac{1}{M}\sum_{m=1}^{M} |e^m_{ij}| \tag{4.9}$$

allows us to assess how close the *ensemble* of configurations is to being TI. In particular we are interested in how $\langle d_{ij}\rangle^N_M$ decreases as we increase the number of fibres N in the periodic cell. In Fig. 5 we use a log scale for N to show how the mean absolute relative errors $\langle d_{66}\rangle^N_{1000}$, $\langle d_{11}\rangle^N_{1000}$ and $\langle d_{44}\rangle^N_{1000}$ depend on N. It is found that the largest anisotropy always occurs for $N = 2$. After $N = 4$ each of the mean errors monotonically decreases as N increases. Furthermore the strictest indicators of transverse isotropy in this context are $\langle d_{66}\rangle$ and $\langle d_{44}\rangle$, which remain largest for longer (as a function of N). Presumably this is due to the large contrast in shear modulus between phases. One must accept, of course, that the (averaged) effective modulus tensor can never be strictly TI when averaged over a finite number of configurations. So, we must always choose a tolerance t_1 (see Fig. 5) for the anisotropy and we are then satisfied when all $\langle d_{ij}\rangle < t_1$. With $t_1 = 0.04$, transverse isotropy on the configurational average is achieved by $N = 3$; with $t_1 = 0.02$ we require $N \sim 16$ and for $t_1 = 0.01$ then $N \sim 64$ is needed.

Analysing the average properties of an ensemble of configurations is an essential measure of how close a fibre-reinforced material is to being TI; however, it is also of interest to consider whether a *single* configuration can be used to predict the effective properties. This would be useful since then the time-consuming configurational averaging would not be required. Therefore, we address the issue posed in question (2c). That is, we must assess the departure from transverse isotropy for a *specific* configuration and in particular we consider how many N are required for that specific configuration to be considered TI, to some given tolerance. Important quantities that allow us to answer this question are (i) the

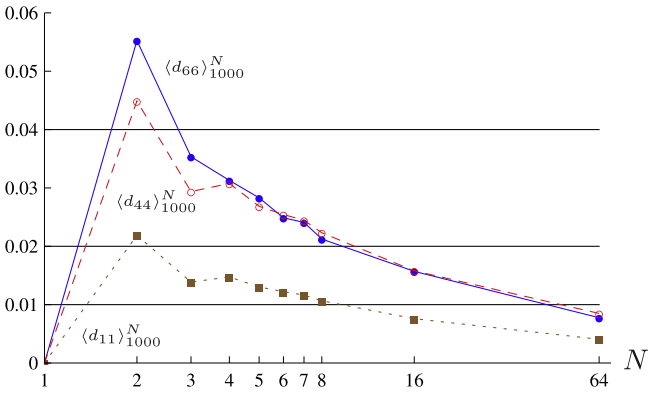

Fig. 5. For a hexagonal periodic cell with $\phi = 0.15$ the mean absolute relative errors $\langle d_{66}\rangle^N_{1000}, \langle d_{11}\rangle^N_{1000}$ and $\langle d_{44}\rangle^N_{1000}$ for a set of 1000 configurations are shown for $N = 1, 2, 3, 4, 5, 6, 7, 8, 16$ and 64. The abscissa represents N using a log-scale. The different tolerances for the anisotropy are $t_1 = 0.01, 0.02$ and 0.04 and are shown by the solid horizontal lines.

spread (variance) of the relative errors defined in (4.8), i.e. the corresponding standard deviation

$$\Sigma^N_{ij\,M} = \sqrt{\frac{1}{M}\sum_{m=1}^{M}\left(\langle e_{ij}\rangle^N_M - e^m_{ij}\right)^2} \tag{4.10}$$

and (ii) the percentage of the e^m_{ij} that are within some tolerance t_2 of the mean value $\langle e_{ij}\rangle$, defined as

$$\%^N_{ij\,M} = \frac{100}{M}\sum_{m=1}^{M} n^m_{ij}, \text{ where } n^m_{ij} = \begin{cases} 1, & \text{if } |\langle e_{ij}\rangle^N_M - e^m_{ij}| < t_2, \\ 0, & \text{otherwise.} \end{cases} \tag{4.11}$$

The former gives a useful measure of how *close* a set of configurations is to being TI, whereas the latter is particularly useful for estimating the likelihood that a single configuration is TI, to within the tolerance required.

Based on our results thus far, it seems likely that we will need a large N for a single configuration to be considered TI (as usual, we consider a hexagonal cell with $\phi = 0.15$ here but note that for smaller ϕ the required N will be lower due to the reduced effect of the fibre material on the composite in these cases). This is, of course, at the heart of the notion of a representative volume element, i.e. provided N is large enough, then only a small number M of realizations are required in order to specify the effective properties of the resulting *random* medium. We focus on the relative error e^m_{66} because we saw in Fig. 5 that this provides the strictest test of transverse isotropy for the composite we are studying.

Before considering the standard deviation $\Sigma^N_{ij\,M}$, let us analyse the distribution of a typical randomly generated set of $M = 1000$ relative errors e^m_{ij}. We take a hexagonal periodic cell with $\phi = 0.15$. In Fig. 6 we plot histograms of these results (for (a) $N = 4$ and (b) $N = 64$) with their associated normal distributions. Note that for these to be compared sensibly we have plotted the *frequency fraction* histograms, i.e. the vertical axis is the frequency divided by Mh where here $M = 1000$ and $h = 0.002$ is the bin width. In both cases the normal distribution appears qualitatively to be a good fit to the data with a noticeable improvement in the case of $N = 64$ as should be expected. We note that the standard deviation decreases as we increase N. We can however, apply a more quantitative analysis of the normality of our results by using the Kolmogorov–Smirnov (KS) test. In Table 3 we state the p-value (significance level) corresponding to the KS test in the case of a sample of 1000 configurations of the composite where the periodic cell contains $N = 2, 4, 16$ and 64 fibres. We see that if we check for 10% statistical significance of normality (a common check in practice), this would be achieved in both the $N = 16$ and 64 cases.

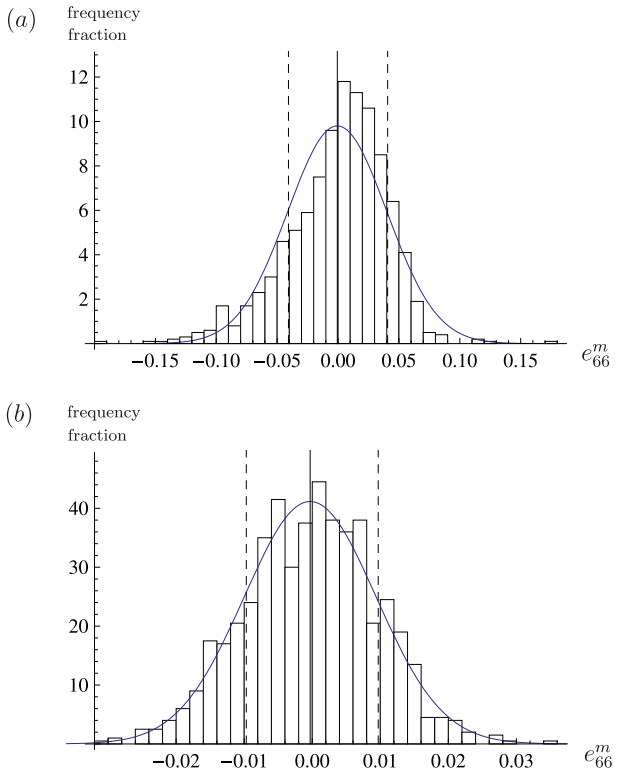

Fig. 6. Histograms to show frequency fraction of occurrence of the different values taken by the relative error e^m_{66} for a set of 1000 different configurations, for a hexagonal periodic cell with fibre volume fraction $\phi = 0.15$ and (a) $N = 4$, (b) $N = 64$. The continuous curve represents a normal distribution with the same mean and standard deviation as the set of relative errors. The solid vertical line represents the mean value and the two dashed vertical lines show the value of one standard deviation either side of the mean.

In Table 4 we present results for Σ^N_{66M} and $\%^N_{66M}$ (to within different values of t_2) for a group of 1000 configurations, for $N = 2, 4, 16, 64$. (For $N = 1$ all configurations are the same so we do not need to consider this case here.)

The standard deviation $\Sigma^N_{66\,1000}$ decreases with increasing N, thus the spread in the range of values of the individual errors e^m_{ij} decreases for increasing N. For the tolerance $t_2 = 0.1$ there is little difference in the choice of N, in other words, the quantity $\%^N_{66M}$ indicates that most configurations are TI to this tolerance. On the other hand, as we decrease the allowable tolerance, variation with N becomes apparent. In particular for $t_2 = 0.01$ around 70% of configurations with $N = 64$ can be classified as TI compared with less than 40% for $N = 16$. We conclude that using $N = 64$ will, in general, lead to the majority of realizations being good approximations of TI materials, especially since $\langle e_{66}\rangle^N_M$ is a strict indicator of transverse isotropy.

It should be reiterated here that the above results are given for this one specific set of 1000 configurations; however, referring to Table 2 it can be concluded that the results are representative of a typical set of this number of configurations.

4.4. Cell shape dependence

Having considered a hexagonal cell in the previous section, we here focus on question (3) of the Introduction: how do the effective properties depend on the shape of the periodic cell? The symmetries of the cell will be exhibited at the macroscale, and so the effective properties associated with any specific configuration must depend on the cell shape; however, the influence of the shape is expected to become negligible as $N \to \infty$. We shall consider the following questions: (i) does each cell shape lead to a transversely isotropic material, in a configurational average sense, for sufficiently large N, and (ii) do the resulting (converged) configurational averaged elastic moduli depend on the cell shape?

In Table 5 we present results for $\langle c^*_{66}\rangle^N_M$ and $\langle d_{66}\rangle^N_M$, for hexagonal, square and rectangular cells with $\phi = 0.15$. Results for other values of ϕ are qualitatively similar. For each of the three cell shapes we normalize the area $|D|$ to be unity so that $\phi = N\pi a^2$ and so as to allow us to compare the results for the different shapes directly. Results for $N = 1, 4, 16$, and 64 are shown. In every case, the maximum departure from a transversely isotropic material (largest error) occurs at $N = 2$. After $N = 4$ the error then decreases monotonically with increasing N as we see in Fig. 5 in the previous subsection. Moreover, the magnitude of the ensemble averaged error is approximately the same for all the cell shapes, but the rate at which the material approaches transverse isotropy appears to be slightly faster for a square or hexagonal cell than a rectangular cell, because of the higher degree of anisotropy that the rectangular shape naturally induces. The configurational averaged elastic modulus appears to be converging, with increasing N, to the same value irrespective of the cell shape. Note that in this table the values of the configurational averages are accurate to 3 decimal places.

It is perhaps worth mentioning that the averaged results in the table are not equal to any of the single-fibre results at the same volume fraction. In other words, assuming that the configurational averaged results are indicative of the actual effective properties of the composite material, a cell containing a single fibre (of the same material and volume fraction) can never exactly reproduce these effective properties. However it can give a good approximation as we show in Table 5. In particular, the hexagonal cell case is very close, with $\langle c^*_{66}\rangle^N_M$ differing by less than 1.2% between the single fibre and 64-fibre periodic cells.

In summary, each cell shape does appear to give a converged configurational averaged *transversely isotropic* elastic modulus tensor for sufficiently large N, and furthermore this tensor is independent of the cell shape.

Table 3
Showing the p-value (significance level) given by the Kolmogorov–Smirnov normality test, corresponding to the level of statistical significance that the sample (with $M = 1000$ is normally distributed. A typical test would check for 10% statistical significance ($p > 0.1$) which is therefore achieved here in the cases of $N = 16$ and $N = 64$.

Number of fibres in cell	p-Value
2	0
4	1.02×10^{-4}
16	0.1165
64	0.7328

Table 4
For a hexagonal cell with $\phi = 0.15$ we show the standard deviation Σ^N_{66M} and the percentage $\%^N_{66M}$ of the deviations e^m_{ij} that lie within different tolerance values t_2 of $\langle e_{66}\rangle^N_M$. Results for a set of 1000 different configurations for each of $N = 2, 4, 16, 64$ are shown.

N	$\Sigma^N_{66\,1000}$	$\%^N_{66\,1000}$			
		$t_2 = 0.1$	$t_2 = 0.01$	$t_2 = 0.005$	$t_2 = 0.001$
2	0.0668	85.8	5.7	2.6	0.7
4	0.0407	97.7	20.8	9.9	1.8
16	0.0199	100	38.6	19.1	5.2
64	0.00969	100	69.4	38.4	8.7

Table 5
Results for the configurational averaged constant $\langle c^*_{66}\rangle^N_M$ and mean absolute relative error $\langle d_{66}\rangle^N_M$ determined for hexagonal, square and rectangular periodic cells, for a set of $M = 1000$ random configurations with $N = 1, 4, 16, 64$ and $\phi = 0.15$.

N	$\langle c^*_{66}\rangle$ hex	$\langle d_{66}\rangle$ hex	$\langle c^*_{66}\rangle$ square	$\langle d_{66}\rangle$ square	$\langle c^*_{66}\rangle$ rect	$\langle d_{66}\rangle$ rect
1	1.264	0	1.233	0	1.213	0
2	1.276	0.0553	1.260	0.0528	1.246	0.0656
4	1.277	0.0313	1.270	0.0331	1.263	0.0468
16	1.279	0.0157	1.277	0.0157	1.276	0.0171
64	1.279	0.00776	1.279	0.00758	1.278	0.00798

4.5. Comparison with other homogenization and micromechanical methods

In this section we consider question (4) of the introduction: to compare results from the periodic cell model with those derived by established methods of homogenization and micromechanics. We shall focus on typical glass–epoxy and boron–aluminium composites for this investigation.

Let us first consider the glass–epoxy composite with properties described at the start of this section. We compute results for the effective properties $\langle c^*_{ij}\rangle^N_M$ averaged over $M = 1000$ configurations at volume fractions $\phi = 0.05, 0.15, 0.25, 0.35$ and we take the case of $N = 64$ fibres within the cell. We inferred in Section 4.2 that as ϕ is increased an increasing number of configurations is needed to get convergence to the same accuracy. Thus, for fixed M, the results for $\phi = 0.05, 0.15$ are accurate to 3 decimal places while the results for $\phi = 0.25, 0.35$ are accurate to 2 decimal places.

We compare our results for each of the square, hexagonal and rectangular periodic cells with (i) the variational bounds of Hashin (1965), determined for a two-phase transversely isotropic fibre-reinforced composite, (ii) the self-consistent results of Hill (1965), and (iii) the multiple scattering theory predictions of Bose and Mal (1974a,b). The latter approach is taken in the low frequency limit, and the pair-correlation function used is that of no interaction between fibres except for no overlap. For ease of exposition, analytic expressions for the elastic moduli, derived by each of these methods, are given in the appendix. Note that in the context of the glass–epoxy composite, where the properties $\mu_1 > \mu_0,\ k_1 > k_0$ (where $k = \lambda + \mu$ is the in-plane bulk modulus) the multiple scattering theory prediction is identical to the *lower* Hashin bound and this can be seen in the Figures below. All of the periodic cell results and the self-consistent results lie below the upper Hashin bound. However, the upper bound c^+_{ij} gives much larger values for the effective properties than any of the other methods shown, so we have omitted this bound in the Figures below for clarity.

In Figs. 7–9 we present results for three effective elastic properties: the in-plane shear modulus c^{eff}_{66}, the axial shear modulus c^{eff}_{44} and the plane strain (in-plane) bulk modulus $k^{eff} = (c^{eff}_{11} + c^{eff}_{12})/2$ as predicted by a number of schemes. Each property is scaled on the appropriate value of the host material so that its magnitude is unity at $\phi = 0$. The results at the volume fractions indicated above are plotted for each periodic cell shape and, as is seen, there is very little difference between these for $N = 64$. These Figures provide us with another opportunity to examine the dependence of the periodic cell method on the choice of the cell shape, this time for a wider range of ϕ values. The Figures confirm our findings from Section 4.4, i.e. that for large enough N there is very little difference in the results for the three different cell shapes, and this is confirmed here for any ϕ value.

This analysis enables us to draw conclusions about the efficacy of the various homogenization techniques. The self-consistent method does favour the lower variational bound for small ϕ, but then deviates significantly from these values as ϕ increases. The periodic cell predictions sit within the Hashin bounds for all ϕ and for all cell shapes and we note that they also favour the lower variational bound. We expect that incorporating a more complex correlation function into the multiple scattering analysis, which

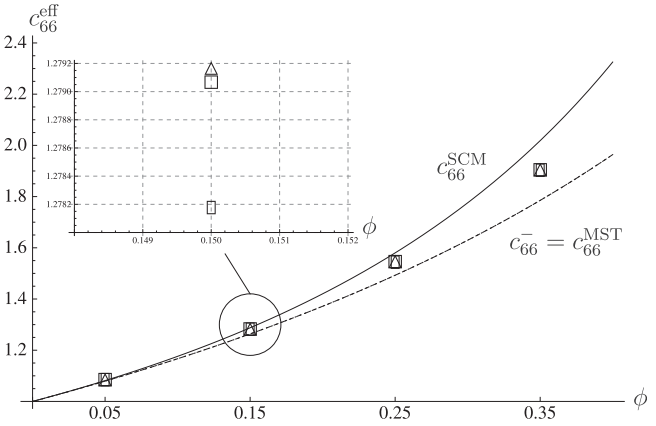

Fig. 7. Results from various methods for the effective in-plane shear modulus c^{eff}_{66} for fibre volume fraction in the range $0 \leqslant \phi \leqslant 0.4$. Our results from the periodic cell method are shown by triangle markers for a hexagonal cell, squares for a square cell and rectangles for a rectangular cell. At $\phi = 0.15$ our periodic cell results are shown in greater detail to highlight the values for the different cell shapes. The lower c^-_{66} variational bound of Hashin (1965) is represented by the dashed lines. The multiple scattering theory prediction of Bose and Mal (1974a,b), $c^{\rm MST}_{66}$, is equal to the lower Hashin bound and is shown by the dotted line. The solid line shows the self-consistent results, $c^{\rm SCM}_{66}$, of Hill (1965).

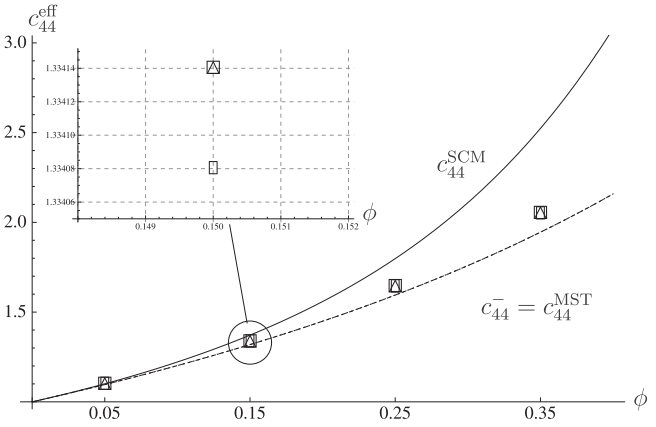

Fig. 8. As in Fig. 7 but with ordinate c^{eff}_{44}.

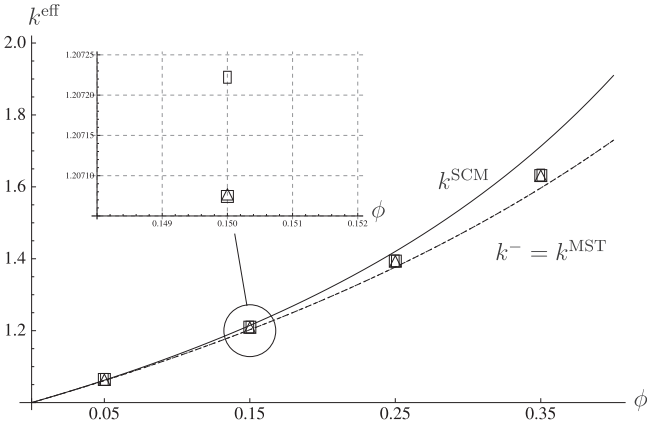

Fig. 9. As in Fig. 7 but with ordinate k^{eff}.

Table 6
Scaled results (to two decimal places) for a Boron/Aluminium composite with $\phi = 0.48$. We show the single fibre ($N = 1$) results from the method of asymptotic homogenization (MAH) for a hexagonal and square cell. In the MST column are the multiple scattering theory predictions from Bose and Mal (1974a,b) and in the SCM column are the self-consistent results of Hill (1965).

c_{ij}	Experimental Datta and Ledbetter (1983)	RVE Hexagon	REV Square	$N = 1$ MAH Hexagonal	$N = 1$ MAH Square	MST	SCM
$k^{eff} = (c_{11}^{eff} + c_{12}^{eff})/2$	1.57	1.52	1.52	1.51	1.51	1.51	1.56
c_{66}^{eff}	1.97	2.05	2.05	2.00	1.78	1.96	2.14
c_{44}^{eff}	2.12	2.18	2.18	2.10	2.11	2.10	2.46

may perhaps be closer to the real correlation in composite media, will shift those results closer to the periodic cell data, although this hypothesis has not yet been tested. It is frequently claimed (see e.g. Linton and Martin (2004)) that the use of the Quasi-Crystalline Approximation (QCA) in multiple scattering theory renders predictions valid in only the small ϕ regime. However, it is demonstrated here that there is good agreement between this theory and the periodic cell results, implying that the QCA may well be a good approximation to effective properties in the quasi-static limit over a wide range of volume fractions.

The results in Figs. 7–9 support the claim in Hill (1965) that the self-consistent method works well for low and intermediate ϕ but that at large volume fractions it may be unreliable for host/inclusion composites. We note that there have been a number of alternative self-consistent methods proposed over the last few decades which appear to give better agreement with experimental results (see Kanaun and Levin, 2008a,b). Hill (1965) also mentions that the self-consistent method is particularly likely to be unreliable at large ϕ when the ratio of the fibre to matrix rigidities is extreme, and this is certainly the case for the glass–epoxy composite which has $\mu_1 = 30$ GPa and $\mu_0 = 1.3$ GPa.

For additional model verification and in particular in order to compare with experimental data, let us now consider a Boron-Aluminium composite with properties $E_1 = 397.9$ GPa, $\nu_1 = 0.129$, $E_0 = 71.5$ GPa, $\nu_0 = 0.341$ which correspond to $\mu_1 = 176.3$ GPa, $\lambda_1 = 61$ GPa, $\mu_0 = 26.7$ GPa, $\lambda_0 = 57$ GPa. The results are compactly displayed in Table 6, where we compare periodic cell values with those from various micromechanical methods and with the experimental results from Datta and Ledbetter (1983), for $N = 100$, $M = 100$ (which enables us to obtain convergence of the averaged results to 2 decimal places) and $\phi = 0.48$.

We see that there is no difference between the RVE results for the hexagonal and square cell (to the accuracy obtained), again confirming that for large enough N the cell shape is unimportant. We can also confirm by comparing with the MAH results in the Table that the configurational averaged values, even for a large N such as $N = 100$, are not the same as either the hexagonal or square cell single-fibre results. The periodic cell method is in reasonable agreement with the experimental results from Datta and Ledbetter (1983), with the agreement being slightly better for c_{44}^{eff} and k^{eff} than for c_{66}^{eff}. As we have already observed in this section, there is good agreement between the multiple scattering theory and the RVE method. In contrast, the self-consistent method may be unreliable for large ϕ and this may explain the difference with the periodic cell results, especially for c_{44}^{eff}.

5. Conclusions

This article has been concerned with the efficacy of using *periodic* fibre-reinforced composites (with N fibres distributed inside a periodic cell) to simulate the behaviour of fully random fibre/host materials. In particular, our aim was to carry out a detailed quantitative study of the effectiveness of this approach as compared with other established methods of homogenization and micromechanics; that is, to answer the questions (1)–(4) posed in the introductory section in order to determine what information a periodic cell should contain so that we can define a representative volume element (RVE). A further aim was to add weight to the predictions given by the established methods in the non-dilute fibre regime.

Section 2 summarised the procedure from Parnell and Abrahams (2006, 2008a) for obtaining the effective material properties for a periodic medium in terms of the solution to certain fundamental cell problems. The latter were then solved by either a multipole or finite element method, motivated by the complex microstructure of the cell. Our investigations considered two different fibre-reinforced materials, both with high fibre/host elastic modulus contrasts: a glass–epoxy composite and boron–aluminium composite. In particular, for the latter case it was possible to compare with known experimental data.

The first point addressed in this article (question (1)) was to estimate how large an ensemble size M was required for a given cell, containing N randomly distributed fibres, for the configurational averaging procedure to converge. Results were illustrated in Fig. 3, and summarised in Table 2; for example, for $N = 64$ and a volume fraction of $\phi = 0.15$, the configurational average properties are accurate to 3 decimal places for $M \sim 350$ configurations.

Question (2a) asked if, given a particular cell shape and volume fraction ϕ, the configurational averaged effective properties $\langle c_{ij}^* \rangle$ depend on N. We found in Section 4.3 that these constants *do* indeed vary with N, but rapidly reach a constant value, to within a given accuracy, for sufficiently large N. This was illustrated in Fig. 4 where it was shown that the difference between the prediction for $\langle c_{66}^* \rangle$ with $N = 16$ and $N = 64$ is indistinguishable by eye.

In question (2b) we wished to determine, for some given ϕ and $N > 1$, how *close* the configurational averaged modulus tensor was to being transversely isotropic (TI). (Except for special cases, it can never be *exactly* TI.) We found that the strictest measures of transverse isotropy were c_{44}^* and c_{66}^* due, for the case considered, to the high contrast in shear between phases. In particular, we chose to investigate the range of values of M and N which satisfy the mean absolute relative error inequality $\langle d_{ij} \rangle_M^N < t_1$, where t_1 was some prescribed tolerance and $\langle d_{ij} \rangle_M^N$ is defined in Eq. (4.9). For example, from Fig. 5, with $M = 1000$ and $t_1 = 0.04, 0.02, 0.01$ we needed $N = 3, 16, 64$ fibres respectively to satisfy this criterion.

The previous questions had addressed averaged properties, but it was also important to consider what could be said about the material with regard to a single configuration (question (2c)) as, in practice, experiments will typically be carried out on just one sample. We wanted to assess what N was required in order to be confident that the material properties for a single sample were TI to a given tolerance. For this we defined a measure $\%_{ij\,M}^N$; i.e. the percentage of configurations (from a sample set of size M) that are individually classed as TI (with the same parameter values), given some tolerance t_2. Results were shown in Table 3. As expected, a cell with small N can be considered TI only with a large tolerance, but this will decrease rapidly as N increases. An approach like this, considering the variance rather than the averaged properties, would be useful for material scientists wishing to assess which combinations of fibres and host material would give the desired

physical property and also the smallest variation in effective properties when the mixing of the phases might result in different fibre distributions. This repeatability in properties would be important when a material scientist might want to know the effective properties of a material a priori before conducting any experiments.

Of specific importance in this paper was the need to assess the influence of cell shape on the configurational averaged effective moduli. This was addressed in Section 4.4, in the answer to question (3), where we showed that provided N was large enough the different cell shapes predicted very similar configurational averaged properties. The results, shown graphically in Figs. 7–9, are in good agreement with other established methods of micromechanics and homogenization, which answered the final question (4) in the introduction. We compared the periodic cell results with variational bounds on effective properties of random media, and with predictions from the self-consistent method and the classical multiple scattering technique. The results from the self-consistent method were seen to diverge from the predictions of the other methods as the volume fraction increased. This is often found to be the case for particulate and fibre composites and it is anticipated that the *generalized* self-consistent method (Christensen and Lo (1979)) would give better agreement. We also showed that the periodic cell method appears to compare favourably with real experimental data (Table 6).

In this paper we focused our studies on fibre volume fractions less than 0.5: we could make concrete conclusions regarding questions (1)–(4) in the introduction by considering this range, by analysing the standard deviation and "tolerance" as in Section 4.2 of the paper. Furthermore, larger fibre volume fractions would require large N due to the packing limit for mono-dispersions. This would in turn yield very small standard deviations (due to the limited possible distributions of fibres) and therefore this would not assist us in answering question (2). As an example of this, as we can see from Table 3, for $\phi = 0.15$ with 64 fibres per cell and a tolerance of 0.01, already 69.4% of the fibre configurations are within this tolerance of the mean TI error value. If ϕ is increased further then the percentage of configurations within this tolerance can only increase. Gomez Alvarez-Arenas et al. (2000) studied volume fractions in the full range $\phi \in [0, 1]$ by considering square particles, thus permitting full packing.

We hope that the questions and results discussed in this paper will prove useful to users of RVE or alternative micromechanical and homogenization schemes, particularly when trying to ascertain the domain of validity or applicability of their predictions. Overall, it is seen that the RVE method offers a computationally effective and accurate approach to obtaining the effective material properties of random fibre-reinforced materials. The authors are currently extending this investigation to fully three dimensional (particulate) composites, and these results will be reported in due course.

Future research could include extending the method to the case of poly-disperse distributions of fibres i.e. fibres in the periodic cell having different shapes, sizes or material parameters. The results for a poly-disperse composite would still lie within variational bounds but would clearly differ from the mono-disperse results. It is difficult to make definite predictions regarding results for poly-dispersions because these would differ greatly depending on for example, the range in the size distribution of the inclusions, and hence we offer no discussion of this here. Fibres of non-circular cross-section could also be studied; elliptical fibres have been considered, for example in Parnell and Abrahams (2006), who showed that this induces anisotropy within the plane of the cross-sections. Gomez Alvarez-Arenas et al. (2000) presented results for composites containing square particles and then discussed the effects of elongating the particles to increase connectivity amongst particles. Finally we note that it would also be of interest to use the RVE method in future research to investigate the behaviour of composites containing non-elastic fibres (for example visco-plastic or elasto-plastic). These composites have been studied previously in the literature, Michel et al., 1999.

Acknowledgements

The authors are grateful to Thales Underwater Systems Ltd, the Smith Institute Industrial Mathematics Knowledge Transfer Network and the Engineering and Physical Sciences Research Council (EPSRC) for the award of an Industrial CASE Studentship for Willoughby. The authors would also like to thank Dr. P.A. Cotterill (Thales Underwater Systems Ltd) and Dr. D.J. Allwright (Smith Institute and University of Oxford) for helpful suggestions and comments.

Appendix A. Alternative homogenization methods

Here we quote some results for the effective elastic constants c_{ij}^{eff} derived from alternative homogenization schemes. For details of their derivation we refer the reader to the original papers. All results relate to fibre-reinforced materials, where all fibres are of circular cross section, isotropic and aligned parallel to the x_3 axis. Results come from three sources: the variational bounds of Hashin (1965) which we will denote by c_{ij}^{-} and c_{ij}^{+} for lower and upper bounds respectively (which we write down here in the case when $\mu_1 > \mu_0$ and the in-plane bulk modulus $k_1 > k_0$, the context considered in this paper); the self consistent results from Hill (1965), denoted by c_{ij}^{SCM}; and the multiple scattering approach (at low-frequency and with a pair-correlation function which assumes no interaction between fibres except that they do not intersect) from Bose and Mal (1974a,b) whose moduli will be denoted by c_{ij}^{MST}. Note that when $\mu_1 > \mu_0,\ k_1 > k_0$ this result is equal to the *lower* Hashin bound. All expressions are written in dimensional form.

Axial shear modulus: c_{44}^{eff}

$$\frac{c_{44}^{+}}{\mu_1} = 1 + \frac{2(\mu_0 - \mu_1)(1-\phi)}{2\mu_1 + (\mu_0 - \mu_1)\phi}, \tag{A.1}$$

$$\frac{c_{44}^{-}}{\mu_0} = \frac{c_{44}^{\mathrm{MST}}}{\mu_0} = 1 + \frac{2(\mu_1 - \mu_0)\phi}{2\mu_0 + (\mu_1 - \mu_0)(1-\phi)}, \tag{A.2}$$

$$\frac{1}{2c_{44}^{\mathrm{SCM}}} = \frac{1-\phi}{c_{44}^{\mathrm{SCM}} - \mu_1} + \frac{\phi}{c_{44}^{\mathrm{SCM}} - \mu_0}. \tag{A.3}$$

In-plane shear modulus: c_{66}^{eff}

$$\frac{c_{66}^{+}}{\mu_1} = 1 + \frac{2(\mu_0 - \mu_1)(\lambda_1 + 2\mu_1)(1-\phi)}{2\mu_1(\lambda_1 + 2\mu_1) + (\mu_0 - \mu_1)(\lambda_1 + 3\mu_1)\phi}, \tag{A.4}$$

$$\frac{c_{66}^{-}}{\mu_0} = \frac{c_{66}^{\mathrm{MST}}}{\mu_0} = 1 + \frac{2(\mu_1 - \mu_0)(\lambda_0 + 2\mu_0)\phi}{2\mu_0(\lambda_0 + 2\mu_0) + (\mu_1 - \mu_0)(\lambda_0 + 3\mu_0)(1-\phi)}, \tag{A.5}$$

$$\frac{(1-\phi)(\lambda_0 + \mu_0)}{\lambda_0 + \mu_0 + c_{66}^{\mathrm{SCM}}} + \frac{\phi(\lambda_1 + \mu_1)}{\lambda_1 + \mu_1 + c_{66}^{\mathrm{SCM}}} = 2\left(\frac{(1-\phi)\mu_1}{\mu_1 - c_{66}^{\mathrm{SCM}}} + \frac{\phi\mu_0}{\mu_0 - c_{66}^{\mathrm{SCM}}}\right). \tag{A.6}$$

In-plane bulk modulus: $k^{eff} = (c_{11}^{eff} + c_{12}^{eff})/2$

$$k^{+} = \lambda_1 + \mu_1 + \frac{(\lambda_1 + 2\mu_1)(\lambda_0 - \lambda_1 + \mu_0 - \mu_1)(1-\phi)}{\lambda_1 + 2\mu_1 + (\lambda_0 - \lambda_1 + \mu_0 - \mu_1)\phi}, \tag{A.7}$$

$$k^{-} = k^{\mathrm{MST}} = \lambda_0 + \mu_0 + \frac{(\lambda_0 + 2\mu_0)(\lambda_1 - \lambda_0 + \mu_1 - \mu_0)\phi}{\lambda_0 + 2\mu_0 + (\lambda_1 - \lambda_0 + \mu_1 - \mu_0)(1-\phi)}, \tag{A.8}$$

$$k^{\mathrm{SCM}} = \left(\frac{(1-\phi)}{\lambda_0 + \mu_0 + c_{66}^{\mathrm{SCM}}} + \frac{\phi}{\lambda_1 + \mu_1 + c_{66}^{\mathrm{SCM}}}\right)^{-1} - c_{66}^{\mathrm{SCM}}, \tag{A.9}$$

References

Aboudi, J., 1989. Micromechanical analysis of composites by the method of cells. Appl. Mech. Rev. 42, 193–221.

Bakhvalov, N., Panasenko, G., 1989. Homogenization: Averaging Processes in Periodic Media. Kluwer, Netherlands.

Baxter, S.C., Hossain, M.I., Graham, L.L., 2001. Micromechanics based random material property fields for particulate reinforced composites. Int. J. Solids Struct. 38 (50–51), 9209–9220.

Benveniste, Y., 1987. A new approach to the application fo the Mori–Tanaka theory in composite materials. Mech. Mater. 6, 147–157.

Bose, S.K., Mal, A.K., 1974a. Axial shear waves in a medium with randomly distributed cylinders. J. Acoust. Soc. Am. 55, 519–523.

Bose, S.K., Mal, A.K., 1974b. Elastic waves in a fiber-reinforced composite. J. Mech. Phys. Solids 22, 217–229.

Byström, J., 2003. Influence of the inclusions distribution on the effective properties of heterogeneous media. Compos. B: Eng. 34, 587–592.

Christensen, R.M., Lo, K.H., 1979. Solutions for effective shear properties in three phase sphere and cylinder models. J. Mech. Phys. Solids. 27, 315–330.

Datta, S.K., Ledbetter, H.M., 1983. Elastic constants of fiber-reinforced boron-aluminium: observation and theory. Int. J. Solids Struct. 19, 885–894.

Demmel, J.W., Eisenstat, S.C., Gilbert, J.R., Li, X.S., Liu, J.W.H., 1999. A supernodal approach to sparse partial pivoting. SIAM J. Matrix Anal. Appl. 20, 720–755.

Drugan, W.J., Willis, J.R., 1996. A micromechanics based nonlocal constitutive equation and estimates of representative volume element size for elastic composites. J. Mech. Phys. Solids 44, 497–524.

Frisch, U., 1968. Wave propagation in random media. In: Bharucha-Reid, A.T. (Ed.), Probabilistic Methods in Applied Mathematics, vol. 1. Academic Press, New York, pp. 75–198.

Ghosh, S., Lee, K., Moorthy, S., 1995. Multiple scale analysis of heterogeneous elastic structures using homogenization theory and Voronoi cell finite element method. Int. J. Solids Struct. 32, 27–62.

Gomez Alvarez-Arenas, T.E., Mulholland, A.J., Hayward, G., Gomatam, J., 2000. Wave propagation in 0-3/3-3 connectivity composites with complex microstructure. Ultrasonics 38, 897–907.

Greengard, L., Helsing, J., 1998. On the numerical evaluation of elastostatic fields in locally isotropic two-dimensional composites. J. Mech. Phys. Solids 46, 1441–1462.

Guenneau, S., Poulton, C.G., Movchan, A.B., 2003. Oblique propagation of electromagnetic and elastic waves for an array of cylindrical fibres. Proc. Roy. Soc. Lond. A 459, 2215–2263.

Guilleminot, J., Soize, C., Kondo, D., Binetruy, C., 2008. Theoretical framework and experimental procedure for modelling mesoscopic volume fraction stochastic fluctuations in fiber reinforced composites. Int. J. Solids Struct. 45, 21, 5567–558.

Gusev, A.A., 1997. Representative volume element size for elastic composites: a numerical study. J. Mech. Phys. Solids 45, 1449–1459.

Gusev, A.A., Hine, P.J., Ward, I.M., 2000. Fiber packing and elastic properties of a transversely random unidirectonal glass/epoxy composite. Comput. Sci. Technol. 60, 535–541.

Hashin, Z., 1965. On elastic behaviour of fibre reinforced materials of arbitrary transverse phase geometry. J. Mech. Phys. Solids 13, 119–134.

Heil, M., Hazel, A.L., 2006. oomph-lib – an object-oriented multi-physics finite element library. In: Schafer, M., Bungartz, H.J. (Eds.), Fluid–Structure Interaction, Lecture Notes on Computational Science and Engineering, vol. 53. Springer, New York, pp. 75–198.

Hill, R., 1963. Elastic properties of reinforced solids: some theoretical principles. J. Mech. Phys. Solids 11, 357–372.

Hill, R., 1965. Theory of mechanical properties of fibre-strengthened materials. III: Self-consistent model. J. Mech. Phys. Solids 13, 189–198.

Huet, C., 1990. Application of variational concepts to size effects in elastic heterogeneous bodies. J. Mech. Phys. Solids 38, 813–841.

Kanaun, S.K., Levin, V.M., 2008a. Self-Consistent Methods for Composites. Static Problems, vol. 1. Springer, Dordrecht.

Kanaun, S.K., Levin, V.M., 2008b. Self-Consistent Methods for Composites. Wave Propagation in Heterogeneous Materials, vol. 2. Springer, Dordrecht.

Kanit, T., Forest, S., Galliet, I., Mounoury, V., Jeulin, D., 2003. Determination of the size of the representative volume element for random composites: statistical and numerical approach. Int. J. Solids Struct. 40, 3647–3679.

Kaßbohm, S., Müller, W.H., Feßler, R., 2006. Improved approximations of Fourier coefficients for computing periodic structures with arbitrary stiffness distribution. Comput. Mater. Sci. 37, 90–93.

Keller, J.B., 1962. Wave propagation in random media. In: Birkhoff, G., Bellman, R., Lin, C.C. (Eds.), Hydrodynamic Stability. American Mathematical Society, New York, pp. 227–246.

Lax, M., 1952. Multiple scattering of waves. II: The effective field in dense systems. Phys. Rev. 85, 621–629.

Linton, C.M., Martin, P.A., 2004. Multiple scattering by random configurations of circular cylinders: Second-order corrections for the effective wavenumber. J. Acoust. Soc. Am. 117, 3413–3423.

Michel, J.C., Moulinec, H., Suquet, P., 1999. Effective properties of composite materials with periodic microstructure: a computational approach. Comput. Methods Appl. Mech. Eng. 172, 109–143.

Mori, T., Tanaka, K., 1973. Average stress in matrix and average elastic energy of materials with misfitting inclusions. Acta Metall. 21, 571–574.

Nemat-Nasser, S., Hori, M., 1999. Micromechanics: Overall Properties of Heterogeneous Materials. North-Holland, Netherlands.

Norris, A.N., 1985. A differential scheme for the effective moduli of composites. Mech. Mater. 4, 1–16.

Ostoja-Starzewski, M., 1997. Random field models of heterogeneous materials. Int. J. Solids Struct. 35, 2429–2455.

Ostoja-Starzewski, M., 2008. Microstructural Randomness and Scaling in Mechanics of Materials. Chapman and Hall/CRC, Boca Raton.

Parnell, W.J., Abrahams, I.D., 2006. Dynamic homogenization in periodic fibre-reinforced media. Quasi-static limit for SH waves. Wave Motion 43, 474–498.

Parnell, W.J., 2007. Effective wave propagation in a pre-stressed nonlinear elastic composite bar. IMA J. Appl. Math. 72, 223–244.

Parnell, W.J., Abrahams, I.D., 2008a. Homogenization for wave propagation in periodic fibre reinforced media with complex microstructure. I - Theory. J. Mech. Phys. Solids 56, 2521–2540.

Parnell, W.J., Abrahams, I.D., 2008b. A new integral equation approach to elastodynamic homogenization. Proc. R. Soc. Lond. A 464, 1461–1482.

Parton, V.Z., Kudryavtsev, B.A., 1993. Engineering mechanics of composite structures. CRC Press, Boca Raton. rectangular order upon the properties of a medium. Philos. Mag. 34, 481–502.

Sab, K., 1992. On the homogenization and the simulation of random materials. Eur. J. Mech. A: Solids 11, 585–607.

Sabina, F.J., Bravo-Castillero, J., Guinovart-Díaz, R., Rodríguez-Ramos, R., Valdiviezo-Mijangos, O.C., 2002. Overall Behaviour of two-dimensional periodic composites. Int. J. Solids Struct. 39, 483–497.

Sabina, F.J., Smyshlyaev, V.P., Willis, J.R., 1989. Self-consistent analysis of waves in a matrix-inclusion composite–I. Aligned spheroidal inclusions. J. Mech. Phys. Solids. 41, 1573–1588.

Shewchuk, J.R., 1996. Engineering a 2D quality mesh generator and delaunay triangulator. In: Lin, M.C., Manocha, D. (Eds.), Applied Computational Geometry: Towards Geometric Engineering, Lecture Notes in Computer Science, vol. 1148, Springer-Verlag, Berlin, pp. 203–222 (from the First ACM Workshop on Applied Computational Geometry).

Smith, D.R., Pendry, J.B., 2006. Homogenization of metamaterials by field averaging. J. Opt. Soc. Am. 23, 391–403.

Swaminathan, S., Ghosh, S., Pagano, N.J., 2006. Statistically equivalent representative volume elements for unidirectional composite microstructures. Part I: Without damage. J. Compos. Mater. 40, 583–604.

Torquato, S., 2002. Random Heterogeneous Materials. Springer, New York.

Trias, D., Costa, J., Mayugo, J.A., Hurtado, J.E., 2006. Random models versus periodic models for fibre reinforced composites. Comput. Mater. Sci. 38, 316–324.

Xu, X.F., Chen, X., 2009. Stochastic homogenization of random elastic multi-phase composites and size quantification of representative volume element. Mech. Mater. 41, 174–186.